STL – 8494-6006-SU-000

22 December 1964

Quarterly Status Report

"THEORETICAL STUDY OF THE COUPLING BETWEEN THE SOLAR WIND AND THE EXOSPHERE"

Prepared for

National Aeronautics and Space Administration
Washington 25, D.C.

Contract No. NASw-698

23 September 1964 to 22 December 1964

Report No. 6

E. L. Scarf

Prepared by
F. L. Scarf

H. C. Corben

Approved by
H. C. Corben
Director
Quantum Physics Laboratory

QUANTUM PHYSICS LABORATORY
PHYSICAL RESEARCH DIVISION

TRW Space Technology Laboratories
One Space Park
Redondo Beach, California

THEORETICAL STUDY OF THE COUPLING BETWEEN THE SOLAR WIND AND THE EXOSPHERE

APPENDIX A

Superthermal Electron Production in the Transition Region*

R. W. Fredricks, F. L. Scarf and W. Bernstein
TRW Space Technology Laboratories

The ion acoustic wave-electron gyrofrequency resonance is examined quantitatively and the results used to discuss the production of $E > 30$ kev electrons in the solar wind-geomagnetic field transition region. The wave is represented by a potential distribution $\phi = \phi_o \sin(\vec{k} \cdot \vec{r} - \omega t + \psi)$ with $0 < \omega < \Omega_p$ (ion), $0 < k <$ k (Debye), and ψ a stochastic phase variable associated with nonlinear effects. It is estimated the $e\phi_o$ may approach 35% of the incident wind energy in localized regions, and sample numerical solutions to the equations of motion are used to show that the maximum electron energy derived from this resonance is of the order of 130 $e\phi_o$. The resonance conditions leading to production of significant (30-80) kev electron fluxes are discussed and some favorable magnetic field configurations are implicitly described.

---

* Transactions, A.G.U., 45, No. 4, 630, December 1964.

THEORETICAL STUDY OF THE COUPLING BETWEEN THE SOLAR WIND AND THE EXOSPHERE

APPENDIX B

A Possible Interpretation of the P-11 VLF Measurements*

F. L. Scarf and R. W. Fredricks
TRW Space Technology Laboratories

The possibility that the large amplitude VLF electric fields detected on the P-11 spacecraft are associated with longitudinal plasma oscillations is considered. In a collisionless plasma, the mode that can be generated most easily is the ion acoustic mode with $E = -\nabla\phi$, $\phi = \phi_o \cos(\vec{k} \cdot \vec{r} - \omega t)$ and $0 < \omega < \Omega_p$ (ion). If $T_e >> T_i$, theory indicates that a very small current should induce growing waves, but laboratory experiments show that the instability occurs even more readily than predicted by the theoretical threshold calculations. These electric field fluctuations allow fast diffusion of charged particles across magnetic fields and thus the presence of ion acoustic waves could be related to electron precipitation and diffusion phenomena observed on Injun 3, Explorer 14, and Air Force satellites. The mechanism for auroral injection may also involve the fast diffusion process.

---

* Transactions, A.G.U., 45, No. 4, 598, December 1964.

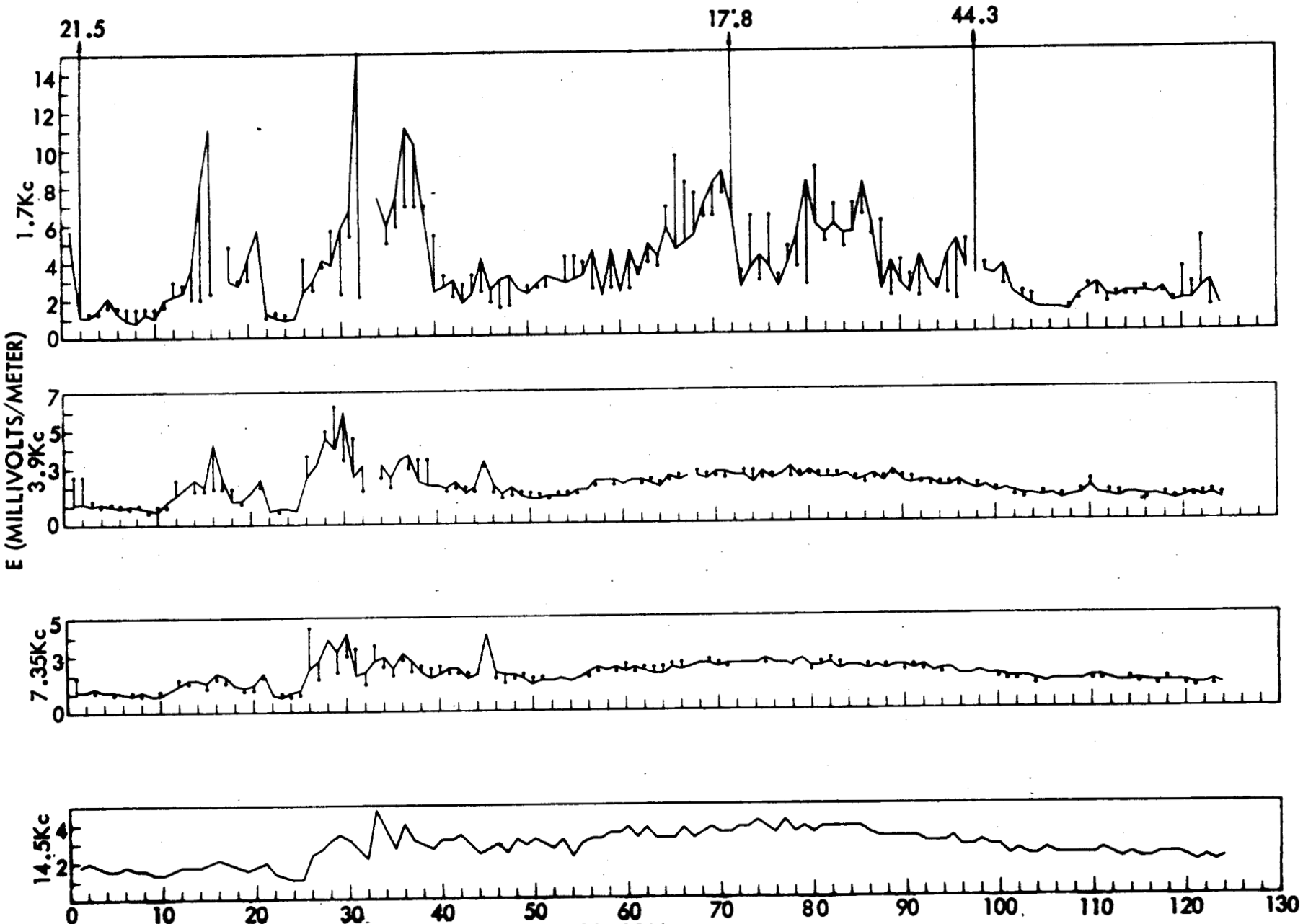

P11, VLF ELECTRIC FIELDS, ORBIT 47, AUGUST 19, 1964
SEQUENCE: 1.7,3.9,7.35, AND CAL, 14.5,7.35,3.9,1.7, OVERCOUNTER, TEMP: REPEATED EVERY 1.068 MINUTES

PREPRINT

THEORETICAL STUDY OF THE COUPLING BETWEEN THE SOLAR WIND AND THE EXOSPHERE

CONDUCTIVE HEATING OF THE SOLAR WIND, II: THE INNER CORONA

F. L. Scarf and L. M. Noble
TRW Space Technology Laboratories, Redondo Beach, Calif.

Abstract

New numerical solutions to the Navier-Stokes equations are used to describe the streaming solar atmosphere. It is argued that no external heat input is needed beyond about $2R_\odot$ if the coronal base temperature is near 1.5×10^6 °K and the plasma has a uniform 10% concentration of helium. In the subsonic region, thermal conduction dominates the flow and viscous effects are unimportant. The transition to supersonic flow occurs near $7R_\odot$, and beyond this radius viscous forces are extremely significant. It is shown that solutions to the inviscid model are singular and that they are not related to the limiting solutions for small, but finite, viscosity.

Submitted to the Astrophysical Journal, November 1964.

1. INTRODUCTION

Recent numerical calculations (Noble and Scarf, 1963; hereafter referred to as I) tend to confirm the hypothesis that the solar wind is a natural extension of the solar corona with thermal conduction beyond a thin shell heating region providing the main local energy flux which induces the supersonic flow. In this series of papers the validity of the conductive heating model is examined in greater detail, and the model is modified and extended. The previous discussion was based on study of a particular solution to a dimensionless form of the Navier-Stokes equations, and viscous dissipation was not explicitly included. These calculations have now been supplemented in two ways: (a) a broad range of solutions is examined in order to determine the best fit to the observed coronal density in the inner region, $R_\odot < r < (8\text{-}10)R_\odot$. As in (I), no external heat source is considered and viscous terms are neglected near the base; (b) viscous corrections are inserted and it is found that they become significant beyond the sonic transition at $r = r_c$ so that subsequent numerical integration must be performed without neglect of these terms. A brief summary of some of these results was recently presented (Scarf and Noble, 1964), and in this paper we wish to describe these refinements in detail.

It will be shown that the inviscid model represents a singular flow pattern, and that the correct flow exhibits extremely large velocity gradients so that the applicability of the Navier-Stokes equations becomes questionable at large distances $\left[(15 - 20)R_\odot\right]$. The final paper in this series will contain an investigation of the breakdown of the Navier-Stokes relations, together with speculation on the transition to a form of modified free molecular flow.

2. THE CONTINUUM EQUATIONS

The solar corona is a fully ionized gas containing approximately 10% helium and 90% hydrogen. This plasma is described by a series of Boltzmann equations for electron, proton and alpha-particle distribution functions, and the equations are strongly coupled by coulomb collision terms. If all species have the same local temperature, T, and the same streaming velocity, $\underset{\sim}{u}$, (i.e., if diffusion effects can be neglected), then the lowest order moments of the distribution functions satisfy the following general equations (Burgers, 1960),

$$\frac{\partial N}{\partial t} + \frac{\partial}{\partial x_i}(Nu_i) = 0 \quad , \tag{1}$$

$$N\frac{\partial u_i}{\partial t} + Nu_k\frac{\partial u_i}{\partial x_k} + \frac{1}{m}\frac{\partial}{\partial x_i}(NkT) + \frac{1}{m}\frac{\partial}{\partial x_k}P_{ik} - Ng_i = 0 \quad , \tag{2}$$

$$\frac{3}{2}\frac{\partial}{\partial t}(NkT) + \frac{3}{2}u_i\frac{\partial}{\partial x_i}(NkT) + \frac{5}{2}NkT\frac{\partial u_i}{\partial x_i} + \frac{1}{2}P_{ik}\epsilon_{ik} + \frac{\partial Q_i}{\partial x_i} = 0, \tag{3}$$

with

$$\epsilon_{ik} = \frac{\partial u_i}{\partial x_k} + \frac{\partial u_k}{\partial x_i} - \frac{2}{3}\delta_{ik}\frac{\partial u_j}{\partial x_j} \quad . \tag{4}$$

Here N is the total number density, $(N_e + N_p + N_\alpha)$, m is the mean mass per particle, Nmg_i is the external force per unit volume, and Q_i, P_{ik} represent sums over all species of higher moments of the distribution functions,

$$Q_i(\underset{\sim}{r},t) = \sum_s^{e,p,\alpha} \frac{1}{2}N_s(\underset{\sim}{r},t)m_s\int \left|\underset{\sim}{v} - \underset{\sim}{u}(\underset{\sim}{r})\right|^2 (\underset{\sim}{v} - \underset{\sim}{u}(\underset{\sim}{r}))_i\, f_s(\underset{\sim}{v},\underset{\sim}{r},t)d^3v \quad , \tag{5}$$

$$P_{ik}(\underset{\sim}{r},t) = \sum_s^{e,p,\alpha} N_s(\underset{\sim}{r},t)\, m_s \int (\underset{\sim}{v} - \underset{\sim}{u}(\underset{\sim}{r}))_i(\underset{\sim}{v} - \underset{\sim}{u}(\underset{\sim}{r}))_k\, f_s(\underset{\sim}{v},\underset{\sim}{r},t))d^3v$$
$$- N(\underset{\sim}{r},t)\, kT(\underset{\sim}{r},t)\,\delta_{ik} \quad . \tag{6}$$

The coupled Boltzmann equations lead to very complex general relations for Q_i, P_{ik} (Burgers, 1960), but these can be considerably simplified if each $f_s(\underset{\sim}{v},\underset{\sim}{r},t)$ is sufficiently close to a stationary local Maxwell-Boltzmann distribution,

$$f_s^{(0)}(\underset{\sim}{v},\underset{\sim}{r}) = N_s(\underset{\sim}{r})\left[\frac{m_s}{2\pi kT(\underset{\sim}{r})}\right]^{3/2} \exp\left\{\frac{-m_s(\underset{\sim}{v} - \underset{\sim}{u}(\underset{\sim}{r}))^2}{2kT(\underset{\sim}{r})}\right\}, \tag{7}$$

and if the gradients of N, T and u are "sufficiently small". Although it will be necessary to return to this definition of "sufficiently small" in a subsequent discussion, we presently assume that in the lower corona the aforementioned conditions are satisfied so that the conventional linear approximations, $\underset{\sim}{Q} = -\kappa\nabla T$, $P_{ik} = -\eta\epsilon_{ik}$, are valid; Eqs. (1) - (3) are then the Navier-Stokes equations for motion of a fluid with a mass density $Nm = \sum N_s m_s$ and a specific heat ratio of 5/3.

The transport coefficients κ, η are evaluated by examining the collision terms in the coupled Boltzmann equations. Chapman (1954) computed κ and η in this way for a fully ionized hydrogen gas, and he noted that the electrons are primarily responsible for thermal conduction while the ions dominate the viscous contribution. For a hydrogen plasma, the Chapman transport coefficients are

$$\kappa_o = 6 \times 10^{-7}\, T^{5/2} \text{ ergs/cm - sec - }^oK \quad , \tag{8}$$

$$\eta_o = 1.2 \times 10^{-16}\, T^{5/2} \text{ gm/cm - sec} \quad . \tag{9}$$

If fact, we are concerned here with a somewhat more complex hydrogen-helium plasma, and it is shown in Appendix I that the viscous coefficient is significantly composition dependent. For a 10% helium admixture η should be

reduced to $0.69\,\eta_0$, and we shall refer to this value as the coronal coefficient of viscosity; the thermal conduction coefficient is essentially independent of mixing ratio and κ can be set equal to κ_0.

It is generally assumed that the coronal flow appears to an inertial observer to be stationary, radial, spherically symmetric, and unaffected by electromagnetic forces, and these simplifications are tentatively adopted here; we also assume that no external heat source is present in the corona so that $\underset{\sim}{g}$ is simply the acceleration of solar gravity. [As in (I), Eqs. (1) — (3) are to be integrated numerically and any discrepancy between the observed and predicted corona and solar wind will be taken to indicate that at least one of the above assumptions is invalid.] For this case, the momentum and energy equations are, respectively,

$$Nmu\,\frac{du}{dr} + \frac{d}{dr}(NkT) + \frac{NGM_\odot m}{r^2} = \frac{4}{3}\,r\,\frac{d\eta}{dr}\,\frac{d}{dr}\left(\frac{u}{r}\right) + \frac{4}{3}\,\eta\,\frac{d}{dr}\left[\frac{1}{r^2}\,\frac{d}{dr}\left(r^2 u\right)\right], \qquad (10)$$

and

$$\frac{mu^2}{2} - \frac{GM_\odot m}{r} + \frac{5}{2}\,kT - \frac{\kappa(T)r^2}{c}\,\frac{dT}{dr} - \frac{4}{3}\,\frac{\eta(T)r^2}{c}\left(u\,\frac{du}{dr} - \frac{u^2}{r}\right) = E\,, \qquad (11)$$

where E and $c = Nur^2$ are constants of motion. It is convenient to introduce dimensionless parameters $\psi = mu^2/kT_o$, $\lambda = GM_\odot m/kT_o r$, $\tau = T/T_o$, $\epsilon = E/kT_o$ (T_o is an arbitrary reference temperature), and Eqs. (10), and (11) may then be rewritten in the form

$$\frac{1}{2}\left(1 - \frac{\tau}{\psi}\right)\frac{d\psi}{d\lambda} = 1 - \frac{2\tau}{\lambda} - \frac{d\tau}{d\lambda} - B\tau^{5/2}\left[\frac{5}{4\tau}\,\frac{d\tau}{d\lambda}\left(\frac{d\psi}{d\lambda} + \frac{2\psi}{\lambda}\right) + \frac{1}{2}\,\frac{d^2\psi}{d\lambda^2} - \frac{1}{4\psi}\left(\frac{d\psi}{d\lambda}\right)^2 - \frac{2\psi}{\lambda^2}\right], \qquad (12)$$

$$\frac{\Psi}{2} - \lambda + \frac{5}{2}\tau + \frac{A}{2}\tau^{5/2}\frac{d\tau}{d\lambda} + \frac{B}{2}\tau^{5/2}\left(\frac{d\psi}{d\lambda} + \frac{2\psi}{\lambda}\right) = \epsilon \quad . \qquad (13)$$

Here

$$A = \frac{2\varkappa(T_o)GM_\odot m}{k^2 T_o c} \quad , \quad B = \frac{2}{3}\frac{\eta(T_o)}{\varkappa(T_o)}\frac{k}{m}A = 0.69B_o \quad .$$

3. THE LOWER CORONA

Since B is very small, (B/A = .0123 for a 10% helium corona) the viscous terms should be negligible wherever the velocity gradients are "moderate", and Eqs. (12), (13) become

$$\frac{1}{2}\left(1 - \frac{\tau}{\psi}\right)\frac{d\psi}{d\lambda} \simeq 1 - \frac{2\tau}{\lambda} - \frac{d\tau}{\lambda} \qquad (14)$$

$$\frac{\Psi}{2} - \lambda + \frac{5}{2}\tau + \frac{A}{2}\tau^{5/2}\frac{d\tau}{d\lambda} \simeq \epsilon \quad . \qquad (15)$$

In (I) it was assumed that this approximation is valid everywhere and the equations were integrated on an IBM 7090 computer inward from the earth to the sun with N_e(1 AU), u(1 AU) and T(1 AU) fixed at 3.4 cm^{-3}, 352 km/sec and 2.77×10^5 °K, respectively (A = 400, $T_o = 2 \times 10^6$ °K). The thermal gradient at the earth was varied until a solution which has $\psi \to \tau$ as $\lambda \to \lambda_c$ was obtained. A power series expansion about this singularity was then used to continue the integration into the subsonic lower corona [in (I), $r_c = 5.25\ R_\odot$, $\tau_c = \psi_c = 0.586$].

The density distribution predicted in this manner is the solid curve labeled "solar wind solution" in Fig. 1, and the dashed curves represent observed equatorial densities (the complete references to the experimental curves are contained in I. In Fig. 3 of Ref. (I), the measured electron

densities were compared with the computed total particle density, $N = 1.9\ N_e$ for 10% helium. The figures in the present paper contain more meaningful comparisons since all densities refer to electrons only.)

The preliminary solar wind density curve in Fig. 1 obviously differs from the experimental curves by at least a constant factor, but the general agreement in slope is reasonable. This must be contrasted with the behavior of the curve labeled "subsonic solution". Here N_e, T and dT/dr at $r = 1.25\ R_\odot$ are fixed at values appropriate for the solar wind expansion, but $u(1.25R_\odot)$ is reduced from its critical or solar wind value $\left[u_{s.w}(1.25R_\odot) = 9.14 \text{ km/sec}\right]$ to 9.04 km/sec. As the fluid moves outward, the new velocity distribution then remains just below the wind profile out to the $\psi_c = \tau_c$ crossover at $r_c = 5.25\ R_\odot$; however, in the subsonic case u(r) then falls very rapidly as r is increased and since Nur^2 is constant, the subsonic N(r) curve develops a very sharp knee near $r = r_c$. Thus, the smooth electron density profiles measured in the lower corona (say, $r \leqslant 10\ R_\odot$) already suggest very strongly that the corona flows continuously in the solar wind mode, rather than in any of the subsonic patterns. [The term "subsonic" is used to designate solutions for which $\psi < \tau$ in the entire lower corona, but we do not exclude the possibility that ψ becomes equal to τ at some great distance from the sun. The critical solution of Fig. 1 has $\epsilon_{s.w.} = 7.826$, and the "subsonic" solution has $\epsilon = \epsilon_{s.w.} - 2.8 \times 10^{-5}$, thus the latter is not a solar "breeze" solution with $\epsilon = 0$. However, as $\lambda \to 0$ $(r \to \infty)$, Eq. (15) yields $\psi/2 + (A/7)\, d(\tau^{7/2})/d\lambda - \epsilon \to 0$ so that, we might conceivably have $\psi(\lambda = 0) = 0$, $\tau \to c\lambda^{2/7}$ with $Ac^{7/2} = 7\epsilon$, in which case the solution would indeed be subsonic everywhere. On the other hand, a very small change

in the initial conditions then yields $\psi \rightarrow \psi_o$, $7(\epsilon - \psi_o/2) = Ac^{7/2}$, and in this more general case ψ becomes greater than τ as $r \rightarrow \infty$; at great distances the apparently subsonic solution to Eqs. (14), (15) with $0 < \epsilon < \epsilon_{s.w.}$ generally develops into a supersonic wind.]

The computed density profile in Fig. 1 is consistently below the observed distributions, and it is of interest to vary the theoretical parameters in order to determine the best fit. The parameters which might be changed are the conduction coefficient A, the mean mass m, the reference temperature T_o, and the coordinates of the crossover point, λ_c and ψ_c.

The relative insensitivity of the predicted density profile to variations in composition (m) and base temperature was discussed in Ref. (I), and it was noted that the observed densities within 2 $R_\odot$ were considerably higher than any computed ones. Table 1 shows that $N_e(r)$ is also roughly independent of the crossover location. Here $N_e(r)$ is computed for a range of $\psi_c - \lambda_c$ combinations with A, T_o and m fixed at 200, 1.5×10^6 °K and 0.62 m_H, respectively. The important result is that although N_e does vary somewhat as ψ_c and λ_c are changed, the observed electron densities are always considerably greater than the predicted values, especially in the region below 2 $R_\odot$.

The main variation in the computed density profile is related to a change in (Nur^2), or alternatively a change in the conductive coefficient, A. In Fig. 2 the extent to which the $N_e(r)$ - curves depend on this parameter is shown [here $\psi_c = 0.586$, and $\lambda_c = 1.365$ (A = 100, 400, 600), $\lambda_c = 1.32$ (A = 200); T_o has been adjusted to give the best fit in each case, and all curves correspond to a uniform 10% helium concentration]. For A = 100,

$T_o = 1.5 \times 10^6$ °K the conductive heating calculation yields an $N_e(r)$ distribution which agrees extremely well with the values obtained by Blackwell (1956) and Michard (1954) in the region $2\ R_\odot < r < (8 - 10)\ R_\odot$. Beyond $(8 - 10)\ R_\odot$ the predicted distribution is somewhat lower than that given by Blackwell, but it is known (Blackwell and Ingham, 1961) that the interpretation of these observations is unreliable beyond about $8\ R_\odot$; it has been suggested (Chapman, 1961) that the densities beyond $8\ R_\odot$ should be reduced, with $N_e(20\ R_\odot)$ shifted to perhaps one quarter of the value shown in Figs. 1, 2. With these comments in mind, it may be stated that there is no definite discrepancy between the distribution predicted by the conductive heating theory and observations in the range $2\ R_\odot < r < 20\ R_\odot$. However, if the reduction factor of four is meaningful, it seems likely that Blackwell's data should be reinterpreted so that $N_e^{obs}(r)$ is <u>less</u> than $N_e^{s.w.}(r)$ ($A = 100$, $T_o = 1.5 \times 10^6$ °K) for $8\ R_\odot < r < 20\ R_\odot$. This would indicate that the solar wind actually flows <u>more rapidly</u> than predicted by the conductive heating theory beyond $8\ R_\odot$.

More positive conclusions can be reached concerning the discrepancy which is found in the shell between the coronal base ($r \simeq 1.06\ R_\odot$) and $(2 - 2.5)\ R_\odot$. Here the density observations are quite accurate, and all parameters (A, m, T_o, λ_c and ψ_c) have been varied in an attempt to reproduce the observations. However, the predictions based on Eqs. (14), (15) cannot be made to agree with the experimentally determined values, and we conclude that Eqs. (10), (11) (viscosity is unimportant here) are not valid below $(2 - 2.5)\ R_\odot$. The simplest possible explanation for this breakdown is that the external hydromagnetic or mechanical energy supply

which maintains the coronal base at a temperature near 1.5×10^6 °K is actually dissipated over the large shell extending between 1.06 $R_\odot$ and $(2 - 2.5)R_\odot$. In this case, Eqs. (10), (11) are incorrect because the presence of an important local power source is omitted. However, while it is undoubtedly true that the external heat source penetrates some finite distance into the corona, several other reasonable processes can invalidate Eqs. (10), (11) in this region, and at present it is impossible to identify the thickness of the heating shell with confidence. For instance, it has been suggested (L. Davis, Jr., private communication) that the filamentary structure and other deviations from spherical symmetry (sunspot associated arches, streamers, etc.) can have an extremely important effect on the flow patterns near the coronal base; outgoing plasma streamers may be accelerated as they flow through magnetic nozzles associated with filaments, and it is therefore unlikely that the base region ($r < 2\ R_\odot$) can be well described by Eqs. (10), (11), even in the absence of an external heating source. The flow pattern may also be distorted by diffusive settling of the helium component leading to a variation in the mean mass with altitude (Parker, 1963). Another correction which might be significant is associated with the weakening of the solar gravity field by centrifugal forces. Near the base of the corona the flow is not radial and $u_\phi(r \to R_\odot) \to \Omega R_\odot \sin\theta$, with $\Omega = 2.94 \times 10^{-6}$ rad/sec. It is not known just how u_ϕ decreases with increasing r, but even during quiet periods $u_\phi(r > R_\odot)$ is certainly greater than the angular momentum conservation limit, $\Omega R_\odot^2 \sin\theta/r$, because of the interaction between the plasma and the general magnetic field

(Parker, 1958; Chapman, 1961; Scarf, 1964); thus, the effective solar gravity field can be distorted by corotation phenomena over a range of several solar radii. On the basis of analysis of Pioneer 5 field and Mariner 2 plasma measurements, Greenstadt (1964) found some observational support for a strong corotation model. The second pair of Vela satellites carry plasma probes with high angular resolution and the preliminary solar wind observations also suggest a significant amount of corotation (S. J. Bame, Private communication). It is likely that all of these effects contribute to the discrepancy near the coronal base.

4. VISCOUS EFFECTS

The search for a best with the conductive heating equations involved adjustment of parameters and numerical integration in the region $R_\odot < r < 20\ R_\odot$. More explicitly, boundary conditions were fixed near the sonic transition $\left[r_c \simeq (5 - 7)\ R_\odot \text{ for the curves in Fig. 2}\right]$, and the numerical integration of Eqs. (14), (15) was carried out in both directions away from the crossover. It might be assumed that as λ tends to zero, τ then automatically vanishes and ψ tends to a constant asymptotic streaming energy.

In fact, the numerical integrations do not always yield the temperature and kinetic energy profiles which are anticipated on simple physical grounds. Typical numerical results are shown in Fig. 3, and it can be seen that $T_2 \to 0$ for $\lambda > 0$, and $T_1(0) > 0$. These anomalous examples have straightforward analytical expressions; for small λ the conductive heating equations, (14), (15) possess supersonic solutions with a variety of asymptotic

forms, some of which are physically unreasonable.

By inspection of Fig. 3, it can be determined that the solution with vanishing temperature at finite $\lambda = \lambda_o$ has $\tau_2 \to (\lambda - \lambda_o)^{2/7}$. This unphysical behavior actually does represent a true numerical solution of Eqs. (14), (15), since the expansion

$$\left.\begin{aligned} \tau &\to c(\lambda - \lambda_o)^{2/7} - 7(\lambda - \lambda_o)^{4/7}/3Ac^{3/2} + \cdots \\ \psi &\to 2(\epsilon - Ac^{7/2}/7) + 2\lambda - 2\tau + \cdots \end{aligned}\right\} \lambda \to \lambda_o , \qquad (16)$$

formally satisfies the coupled equations for all c. Similarly, the curves with finite temperature at infinity appear to correspond to the set with asymptotic solutions

$$\left.\begin{aligned} \tau^{7/2} &\to \tau_\infty^{7/2} + \frac{7}{5}\tau_\infty^{5/2}\lambda + (14\,\tau_\infty/A)\lambda \ln \lambda + \cdots \\ \psi &\to c(\epsilon, \tau_\infty) - 4\,\tau_\infty \ln \lambda + \cdots \end{aligned}\right\} \lambda \to 0. \qquad (17)$$

However, the continuous family of physical solutions must have $\tau(\lambda = 0) = 0$, and this generally involves

$$\left.\begin{aligned} \tau &\to c\lambda^{2/7} + (77/9Ac^{3/2})\lambda^{4/7} + \cdots \\ \psi &\to 2(\epsilon - Ac^{7/2}/7) + 2\lambda - 16\tau + \cdots \end{aligned}\right\} \lambda \to 0 \quad . \qquad (18)$$

We regard Eq. (18) as the acceptable physical family of solutions to describe an inviscid fluid with streaming and conductive energy transport which both remain finite at infinity. Parker's analytical studies of Eqs. (14), (15) (1964 a, b; 1965) have been based on the assumption that Eq. (18) with arbitrary c is the correct description of the flow in the small λ

region. In fact, Eqs. (14), (15) admit another special asymptotic behavior for the particular case in which the asymptotic energy transport is purely kinetic (Whang and Chang, 1964); i.e.,

$$\left.\begin{aligned} \tau &\longrightarrow (35\,\lambda/2A)^{2/5} + \cdots \\ \psi &\longrightarrow 2\epsilon + 2\lambda - 12\tau + \cdots \end{aligned}\right\} \lambda \to 0 \quad . \tag{19}$$

This overabundance of asymptotic forms indicates that difficulties can be encountered when a numerical integration of Eqs. (14), (15) proceeds in the direction of decreasing λ . However, Eqs. (16) - (19) illustrate a more significant physical fact; since Eqs. (14), (15) possess unreasonable solutions, the equations themselves cannot represent an adequate description of a physical fluid.

It is not difficult to identify the unphysical aspect of Eqs. (14) and (15) because no real fluid can have a vanishing Prandtl number. The existence of anomalous solutions to the inviscid equations indicates that viscous effects must indeed be significant so that the full Navier-Stokes equations (12, 13) should be retained.

By attempting to treat the viscous terms in Eqs. (12, 13) as a small perturbation, we have determined that these corrections do remain negligible below the sonic transition point, (i.e., $\lambda > \lambda_c$). At $\lambda \approx \lambda_c$ the viscous contribution to the energy equation begins to be significant (on the order of a few percent of the thermal energy), and we therefore carry out all subsequent calculations using Eqs. (14), (15) for $\lambda \geq (\lambda_c - \delta)$ and Eqs. (12), (13) for $\lambda < (\lambda_c - \delta)$; the results are not sensitive to the precise value

for δ if $(\delta / \lambda_c) << 1$, and this approximation allows one to use the simple techniques developed in (I) for treating inviscid flow near the sonic transition.

The dimensionless viscous coefficient appropriate for a 10% helium corona with A = 200 is B = 2.46. The heavy curve in Fig. 4 shows the streaming energy profile obtained by numerical integration of the complete hydrodynamic equations, including uninhibited viscosity beyond the transition near 7.5 $R_\odot$ (T_o = 1.5 x 10^6 °K). The dashed curve with B ≡ 0 is the original solution without viscosity; and the temperature curves are essentially independent of B in this region. The most striking aspects of these calculations are (1) the fact that the streaming energy profile is greatly changed in magnitude by the inclusion of viscosity with $u^2(20\ R_\odot,\ B = 2.46) > 2\ u^2(20\ R_\odot,\ B \equiv 0)$; (2) the observation that the viscous term appears to operate in the wrong direction by yielding a local speed which is greater, not less, than that obtained when viscosity is ignored.

In order to investigate the origin of the second effect, numerical integrations of the Navier-Stokes equations were repeated using artificial enhanced and inhibited values for the viscous coefficient (B = 0.1, 1.0, 3.56). The effect of this variation in B is also shown in Fig. 4 (all other parameters and boundary values remain the same). It can be seen that as B is increased from 0.1 to 3.56, the streaming energy at any given radius is reduced as might be anticipated. Larger viscous dissipation does indeed produce lower flow speeds relative to the sun. However, it is also clear from Fig. 4 that the flow pattern with B ≡ 0 is completely

unrelated to that obtained in the limit $B \rightarrow 0$.

From a mathematical point of view, the fact that $B \equiv 0$ is a singular limit is not difficult to understand. The coupled Navier-Stokes equations are solved by formally writing Eq. (13), for instance, in the form

$$\frac{d\psi}{d\lambda} = \frac{L(\psi, \tau, d\tau/d\lambda, \lambda, A, \epsilon)}{B} \quad , \tag{13a}$$

and this display already casts doubt on the relevance of the inviscid energy equation. A similar situation occurs when one examines the limit $A \rightarrow 0$ for the inviscid model. For instance, Eq. (15) has the form

$$\frac{d\tau}{d\lambda} = \frac{L'(\psi, \tau, \lambda, \epsilon)}{A} \quad , \tag{15a}$$

and the acceptable solutions [Eqs. (18), (19)] have temperature expansions in A^{-1} which obviously become meaningless in the limit $A \rightarrow 0$; these conductive heating solutions are <u>not</u> related to the bounded adiabatic solution of Eqs. (14), (15) with $A \equiv 0$. By the same token, it appears that Fig. 4 merely illustrates that fluid flow with a small amount of viscous dissipation differs greatly from inviscid flow. This conclusion is a familiar one to workers in aerodynamics.

We adopt the solutions with $B/A = .0123$ as the correct ones for the solar corona in the regions where the Navier-Stokes equations are applicable. The related increase in the local streaming speed requires a corresponding reduction in N with $N(r,B)\, u(r,B) = N(r,0)\, u(r,0)$ since the same value for the constant (Nur^2) was used throughout. This means that the predicted

values for $N_e(r)$ should be lower than those shown in Fig. 2. At $r \simeq (7\text{-}10)R_\odot$ no significant reduction is needed but $N_e(r,B)/N_e(r,0) \simeq 0.77$ at $r = 15\ R_\odot$, 0.61 at 20 $R_\odot$, etc. These changes increase the discrepancy between the predicted $N_e(r)$ curves and Blackwell's original results in the uncertain region $(10\text{-}20)R_\odot$, however, the best theoretical curve is now brought into closer agreement with the corrected density profile discussed by Chapman. It is hoped that better density measurements for the region $(10\text{-}20)R_\odot$ will be available in the near future so that more meaningful comparisons can be made.

5. CONCLUSIONS

It has been shown that in the region between 2 $R_\odot$ and 15 $R_\odot$, where reasonably accurate density measurements are available, the solar corona can be well described by the conventional Navier-Stokes equations with no external heat source. The best fit to $N_e(r)$ is obtained for a 10% helium corona with $T_o \simeq 1.5 \times 10^6$ °K, A = 100, B = .0123. Some representative numerical values for this solution are given in Table 2, and it can be seen that the streaming speed increases very rapidly beyond the sonic transition near 7 $R_\odot$. This strong acceleration in the region (10-15) $R_\odot$ is a consistent feature of the full Navier-Stokes equations, but it is not obtained for the singular and unphysical case of zero viscosity. Beyond 15 $R_\odot$, the velocity gradients are so steep that the Navier-Stokes formalism becomes questionable. This problem will be discussed in more detail in the final paper of this series.

Below 2 $R_\odot$ there appears to be a genuine and significant discrepancy between the predictions of the idealized theoretical models and observation.

This suggests that one or more of our assumptions (spherical symmetry, uniform composition, no corotation, no external heat source) is invalid in the coronal base region.

ACKNOWLEDGEMENTS

We are indebted to Dr. E. N. Parker for many stimulating discussions. This work was supported in part by the National Aeronautics and Space Administration under Contract NASw-698.

APPENDIX A

Viscous Coefficient for a Hydrogen-Helium Mixture

The viscous transport coefficient for fully ionized hydrogen has been evaluated by Chapman (1954), who points out that the electrons do not appreciably affect the viscous energy transport due to their small mass. The appropriate moments of the Boltzmann equation for a mixture of fluids are discussed by Burgers (1960). In this appendix Burgers' equations are applied to a mixture of 90% hydrogen - 10% helium. The effect of electrons is not explicitly included.

Burgers' Eq. (5 - 34) is just the i-j moment of the Boltzmann equation in concenient form. The usual linear relation between viscous stress and strain is obtained by neglecting time derivatives and gradients; the resulting equations for a proton-alpha particle mixture are the following:

$$N_p kT\,\epsilon^{ij} = -\frac{\sqrt{2}}{5} N_p\, a_p\, Z_{pp}^{(22)}\, P_p^{ij} - \frac{2}{5} N_p\, N_\alpha\, \alpha\, Z_{p\alpha}^{(22)} \left[\frac{m_\alpha^2}{(m_p + m_\alpha)^2} \frac{P_p^{ij}}{N_p} + \frac{m_p\, m_\alpha}{(m_p + m_\alpha)^2} \frac{P_\alpha^{ij}}{N_\alpha} \right] - \frac{4}{3} N_p\, N_\alpha\, \alpha \frac{m_p\, m_\alpha}{(m_p + m_\alpha)^2} Z_{p\alpha}^{(11)} \left[\frac{P_p^{ij}}{N_p} - \frac{P_\alpha^{ij}}{N_\alpha} \right] \qquad \text{(A-1)}$$

$$N_\alpha kT\epsilon^{ij} = -\frac{\sqrt{2}}{5} N_\alpha\, a_\alpha\, Z_{\alpha\alpha}^{(22)}\, P_\alpha^{ij} - \frac{2}{5} N_p\, N_\alpha\, \alpha\, Z_{\alpha p}^{(22)} \left[\frac{m_p^2}{(m_p + m_\alpha)^2} \frac{P_\alpha^{ij}}{N_\alpha} + \frac{m_p\, m_\alpha}{(m_p + m_\alpha)^2} \frac{P_p^{ij}}{N_p} \right] - \frac{4}{3} N_p\, N_\alpha\, \alpha \frac{m_p\, m_\alpha}{(m_p + m_\alpha)^2} Z_{\alpha p}^{(11)} \left[\frac{P_\alpha^{ij}}{N_\alpha} - \frac{P_p^{ij}}{N_p} \right] . \qquad \text{(A-2)}$$

Here the subscripts p and α refer to protons and alpha particles respectively, P^{ij} and ϵ^{ij} are the viscous stress and strain tensors, respectively, and

$$a_p^2 = \frac{2kT}{m_p} \quad , \quad a_\alpha^2 = \frac{2kT}{m_\alpha} \quad , \quad \alpha^2 = \frac{2kT}{\left(\frac{m_p\, m_\alpha}{m_p + m_\alpha}\right)} \quad .$$

The Z functions are appropriate integrals of the collision cross sections; they are evaluated by Burgers for Coulomb interactions. The following particular integrals are useful here:

$$Z_{pp}^{(11)} \equiv Z = 2\sqrt{\pi}\left(\frac{e_p^2}{kT}\right)\log \Lambda \quad ; \quad \Lambda = \frac{3kT}{e^2}\left[\frac{kT}{4\pi(N_p\, e_p^2 + N_\alpha\, e_\alpha^2 + N_e\, e_e^2)}\right]^{\frac{1}{2}}$$

$$Z_{pp}^{(22)} = 2Z, \quad Z_{\alpha p}^{(11)} = 4Z, \quad Z_{\alpha p}^{(22)} = 8Z, \quad Z_{\alpha\alpha}^{(22)} = 32Z \quad .$$

Inserting these expressions, one can solve Eqs. (A-1) and (A-2) simultaneously, eliminating ϵ^{ij}, to obtain

$$A(f) \equiv \frac{P_\alpha^{ij}}{P_p^{ij}} = \frac{\frac{2\sqrt{2}}{5} + \left[\frac{16}{5}\left(\frac{m_\alpha}{m_p + m_\alpha}\right)^{3/2} + \frac{16}{3}\,\frac{m_p\, m_\alpha^{\frac{1}{2}}}{(m_p + m_\alpha)^{3/2}}\right] f + \frac{32}{15}\,\frac{m_p\, m_\alpha^{\frac{1}{2}}}{(m_p + m_\alpha)^{3/2}}}{\frac{32\sqrt{2}}{5}\left(\frac{m_p}{m_\alpha}\right)^{\frac{1}{2}} + \left[\frac{16}{5}\,\frac{m_p^2}{m_\alpha^{\frac{1}{2}}(m_p + m_\alpha)^{3/2}} + \frac{16}{3}\,\frac{m_p\, m_\alpha^{\frac{1}{2}}}{(m_p + m_\alpha)^{3/2}}\right]\frac{1}{f} + \frac{32}{15}\,\frac{m_p\, m_\alpha^{\frac{1}{2}}}{(m_p + m_\alpha)^{3/2}}} \qquad \text{(A-3)}$$

where $f = \frac{N_\alpha}{N_p}$.

The usual coefficient of viscosity for such a mixture is defined by

$$P_p^{ij} + P_\alpha^{ij} = \eta\,\epsilon^{ij} = P_p^{ij}\left[1 + A(f)\right] \quad . \qquad \text{(A-4)}$$

One can rewrite Eq. (A-1) as follows:

$$\frac{kT}{Za_p}\,\epsilon^{ij} = -\,p_p^{ij}\left\{\frac{2\sqrt{2}}{5} + \left[\frac{16}{5}\left(\frac{m_\alpha}{m_p + m_\alpha}\right)^{3/2} + \frac{16}{3}\,\frac{m_p\, m_\alpha^{\frac{1}{2}}}{(m_p + m_\alpha)^{3/2}}\right] f - \frac{32}{15}\,A(f)\,\frac{m_p\, m_\alpha^{\frac{1}{2}}}{(m_p + m_\alpha)^{3/2}}\right\}. \tag{A-5}$$

For a pure hydrogen plasma one has simply

$$\eta_o = \frac{\frac{kT}{a_p Z}}{\frac{2\sqrt{2}}{5}}\,. \tag{A-6}$$

Combining Eqs. (A-4), (A-5) and (A-6) yields finally

$$\eta = \frac{\eta_o\left[1 + A(f)\right]}{1 + \frac{5}{2\sqrt{2}}\left\{\left[\frac{16}{5}\left(\frac{m_\alpha}{m_p + m_\alpha}\right)^{3/2} + \frac{16}{3}\,\frac{m_p\, m_\alpha^{\frac{1}{2}}}{(m_p + m_\alpha)^{3/2}}\right] f - \frac{32}{15}\,\frac{m_p\, m_\alpha^{\frac{1}{2}}}{(m_p + m_\alpha)^{3/2}}\,A(f)\right\}}\,. \tag{A-7}$$

For the case of interest here, $m_\alpha = 4m_p$ and $f = \frac{1}{9}$. From Eq. (A-3) one then obtains $A(f) = 0.089$. Inserting these values in Eq. (A-7) yields for a 90% hydrogen - 10% helium mixture the result $\eta = 0.69\eta_o$.

TABLE 1. The variation of the density profiles with changes in crossover location ($\lambda_c = GM_\odot m/kT_o r_c$) and energy ($\Psi_c = mu_c^2/kT_o$). The tabular entries represent electron density (cm^{-3}) and these results are all derived using Eqs. (14), (15) with A = 200, $m = 0.62\ m_p$ and $T_o = 1.5 \times 10^6\ ^oK$.

	$\Psi_c = 0.585$		$\lambda_c = 1.365$	
$r/R_\odot$	$\lambda_c = 1.32$	$\lambda_c = 1.40$	$\Psi_c = 0.54$	$\Psi_c = 0.62$
1.6	4.61×10^6	3.38×10^6	3.49×10^6	4.40×10^6
2.0	1.39×10^6	1.09×10^6	1.16×10^6	1.32×10^6
4.5	5.45×10^4	5.05×10^4	5.31×10^4	5.20×10^4
6.8	1.58×10^4	1.51×10^4	1.60×10^4	1.50×10^4
7.2	1.34×10^4	1.28×10^4	1.36×10^4	1.27×10^4

TABLE 2. The best fit solution to the Navier-Stokes equations in the region $2R_\odot < r < 15R_\odot$. This solution ($m = .62\ m_p$, $A = 100$, $B = 1.23$, $T_o = 1.5 \times 10^6$ °K) has a sonic crossover near $7.25\ R_\odot$. Viscous effects are significant only beyond the crossover radius and the Navier-Stokes equations become questionable beyond $15\ R_\odot$.

$r/R_\odot$	u(km/sec)	$N_e(cm^{-3})$	$T(^oK)$
2	18.4	2.03×10^6	1.47×10^6
4.5	72.4	1.02×10^5	1.03×10^6
6.8	105	3.09×10^4	8.89×10^5
7.2	110	2.62×10^4	8.73×10^5
10	146	1.02×10^4	7.92×10^5
12.6	190	4.95×10^3	7.55×10^5
15	246	2.70×10^3	7.35×10^5

REFERENCES

Blackwell, D. E., 1956, M.N., 116, 50.

Blackwell, D. E. and Ingham, M. F., 1961, M.N., 122, 129.

Burgers, J. M., 1960, Plasma Dynamics, ed. F. H. Clauser, (Reading, Mass: Addison-Wesley Publishing Co.).

Chapman, S., 1954, Ap. J., 120, 151.

Chapman, S., 1961, Space Astrophysics, ed. W. Liller (New York: McGraw-Hill Book Co.).

Greenstadt, E. W., 1964, to be published.

Michard, R., 1954, Ann. d'Ap., 17, 429.

Noble, L. M. and Scarf, F. L., 1963, Ap. J., 138, 1169.

Parker, E. N., 1958, Ap. J., 128, 664.

Parker, E. N., 1963, The Solar Corona, ed. J. W. Evans (New York: Academic Press).

Parker, E. N., 1964, Ap. J., 139, 72, 93.

Parker, E. N., 1965, Ap. J., to be published.

Scarf, F. L. and Noble, L. M., 1964, AIAA Journal, 2, 1158.

Scarf, F. L., Space Physics, ed. D. P. LeGalley and A. Rosen, (New York: John Wiley).

Whang, Y. C. and Chang, C. C., 1964, to be published.

FIGURE CAPTIONS

Figure 1. Comparison between sample predictions of the conductive heating equations (no viscosity) and observed electron densities in the inner corona. The references to the experimental papers are contained in (I). The theoretical curve labeled "solar wind solution" represents the density profile for flow which becomes supersonic in the neighborhood of $5R_\odot$. The "subsonic solution" then represents flow in which the energy per particle is reduced by about one part in 10^5; beyond $5R_\odot$ the subsonic speed falls rapidly so that the density becomes large.

Figure 2. Effect of varying A and T_o in the conductive heating equations. Beyond about $8R_\odot$ the A = 100 predicted density is somewhat below the observed curve (Blackwell, 1956) but the interpretation of the measurements is not reliable in this region. The discrepancy for $r < (2\text{-}2.5)R_\odot$ probably represents the appearance of complexities which invalidate the model, as described in the text.

Figure 3. Typical anomalous solutions of the inviscid model equations. These solutions are described by Eqs. (16), (17).

Figure 4. Effect of viscosity on coronal flow. The heavy curve with B = 2.46 (A = 200) represents the streaming for a 10% helium corona. The dashed curve (B = 0) is the corresponding solution for a hypothetical non-viscous fluid; the temperature is essentially independent of η (or B) in this region. The solutions for artificial values of viscosity (B = 0.1, 1.0, 3.56) are

included to illustrate that the limiting flow for small B is unrelated to the singular result obtained with no viscosity.

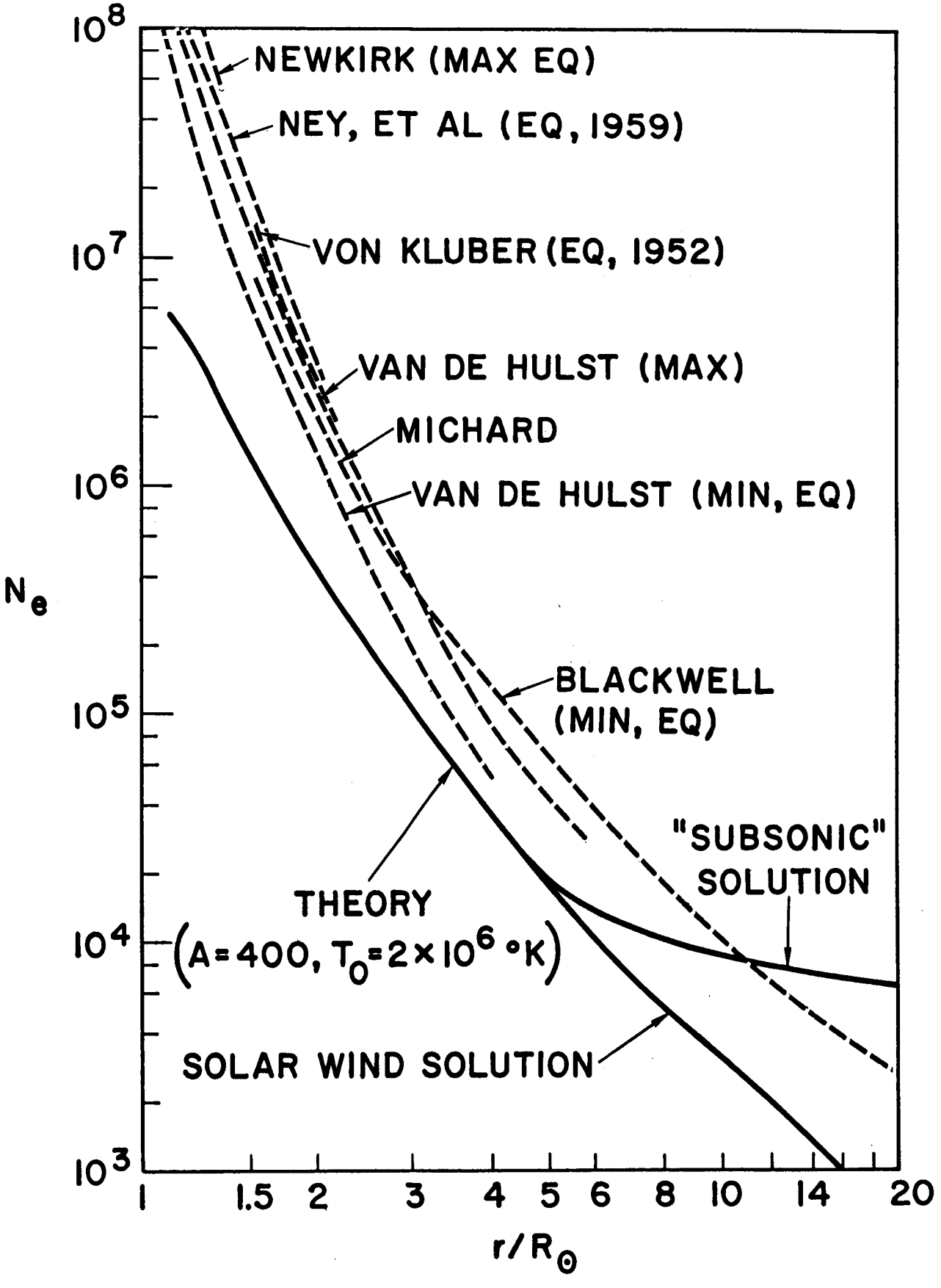
10^8
10^7
10^6
10^5
10^4
10^3
N_e
NEWKIRK (MAX EQ)
NEY, ET AL (EQ, 1959)
VON KLUBER (EQ, 1952)
VAN DE HULST (MAX)
MICHARD
VAN DE HULST (MIN, EQ)
BLACKWELL (MIN, EQ)
"SUBSONIC" SOLUTION
THEORY
(A=400, $T_0=2\times10^6$ °K)
SOLAR WIND SOLUTION
1
1.5
2
3
4
5
6
8
10
14
20
$r/R_\odot$

Figure 1.

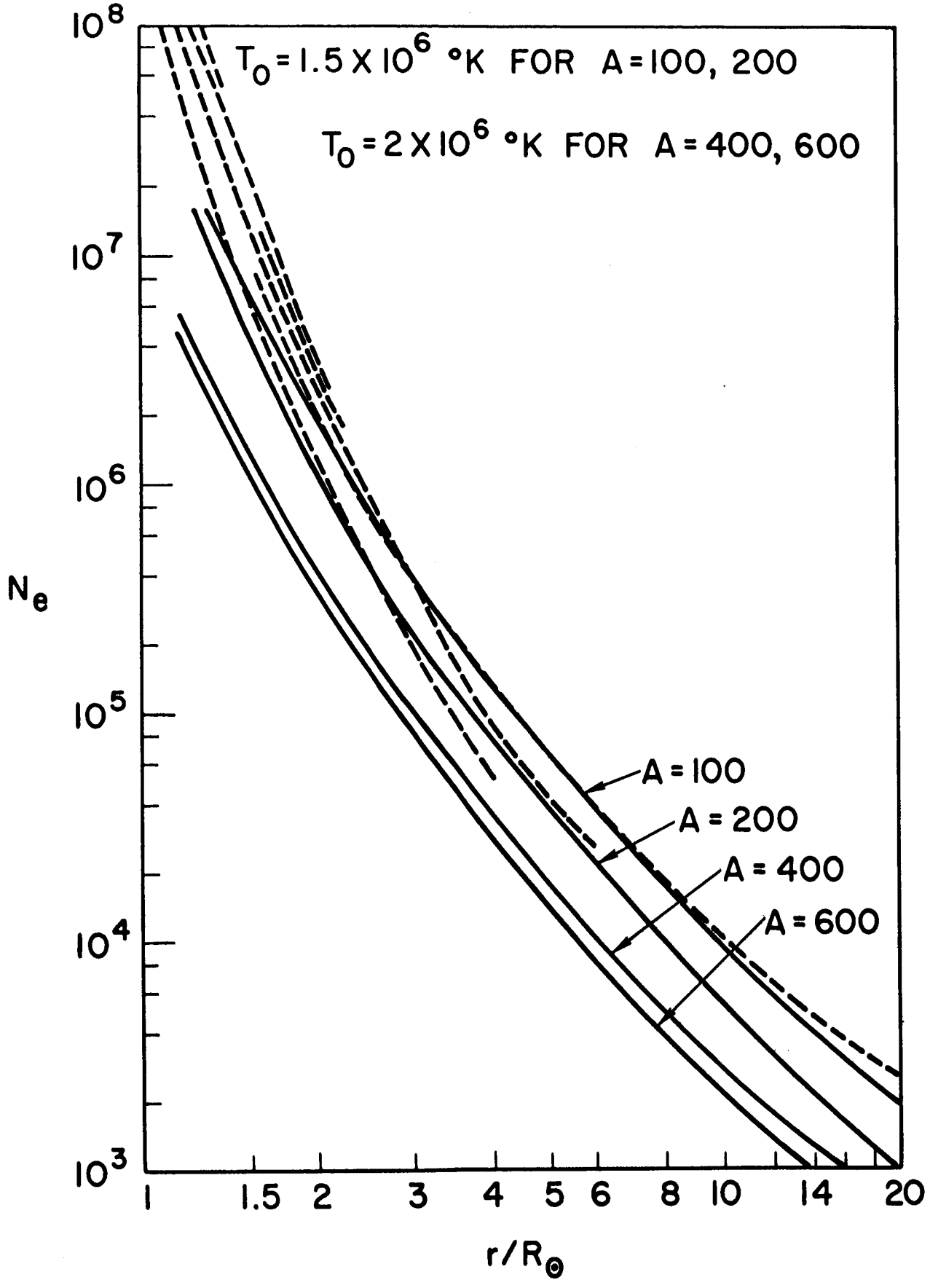
$T_0 = 1.5 \times 10^6$ °K FOR A = 100, 200
$T_0 = 2 \times 10^6$ °K FOR A = 400, 600
10^8
10^7
10^6
10^5
10^4
10^3
N_e
A = 100
A = 200
A = 400
A = 600
1
1.5
2
3
4
5
6
8
10
14
20
$r/R_\odot$

Figure 2.

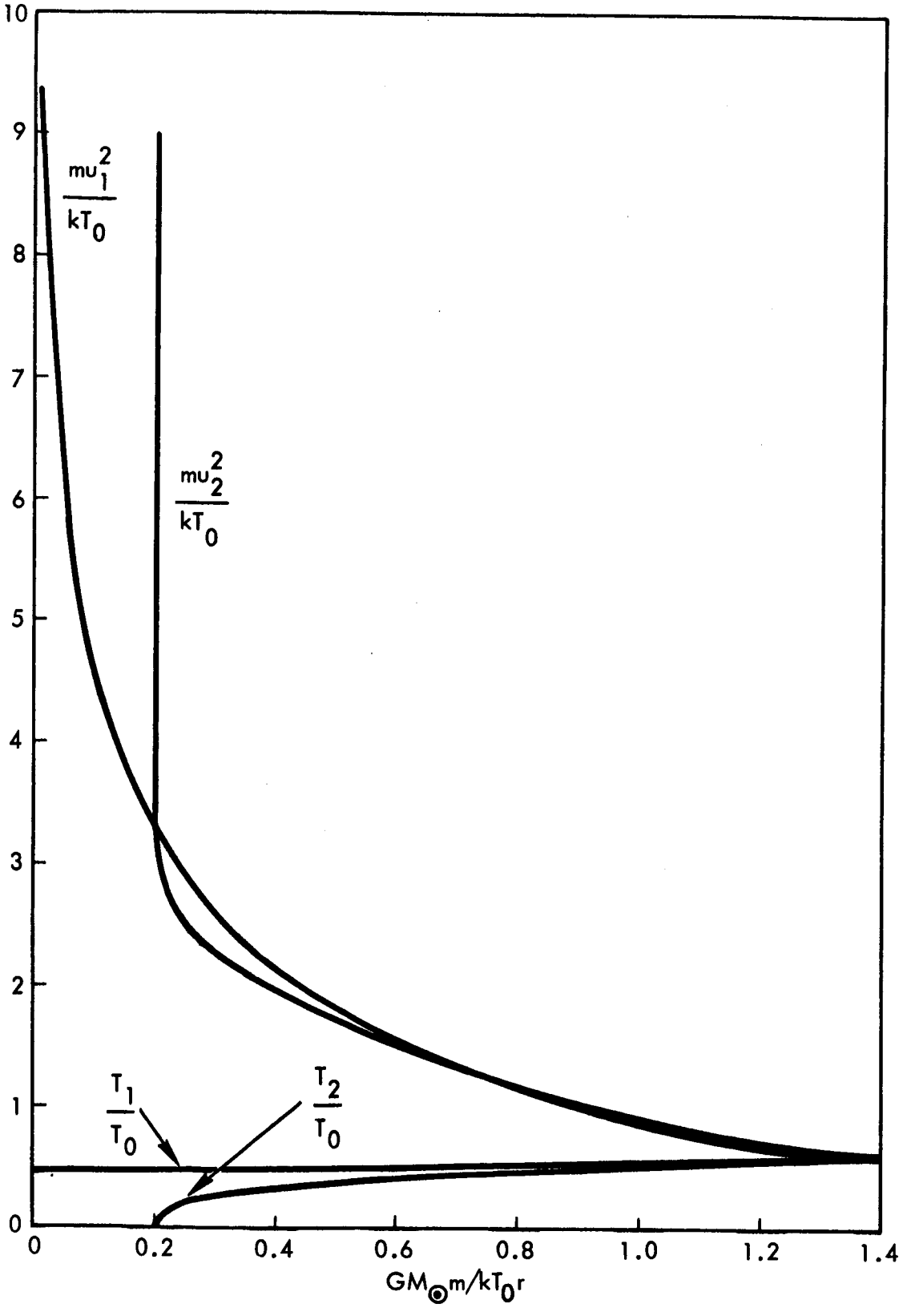
10
9
8
7
6
5
4
3
2
1
0
$\frac{mu_1^2}{kT_0}$
$\frac{mu_2^2}{kT_0}$
$\frac{T_1}{T_0}$
$\frac{T_2}{T_0}$
0
0.2
0.4
0.6
0.8
1.0
1.2
1.4
$GM_\odot m/kT_0 r$

Figure 3.

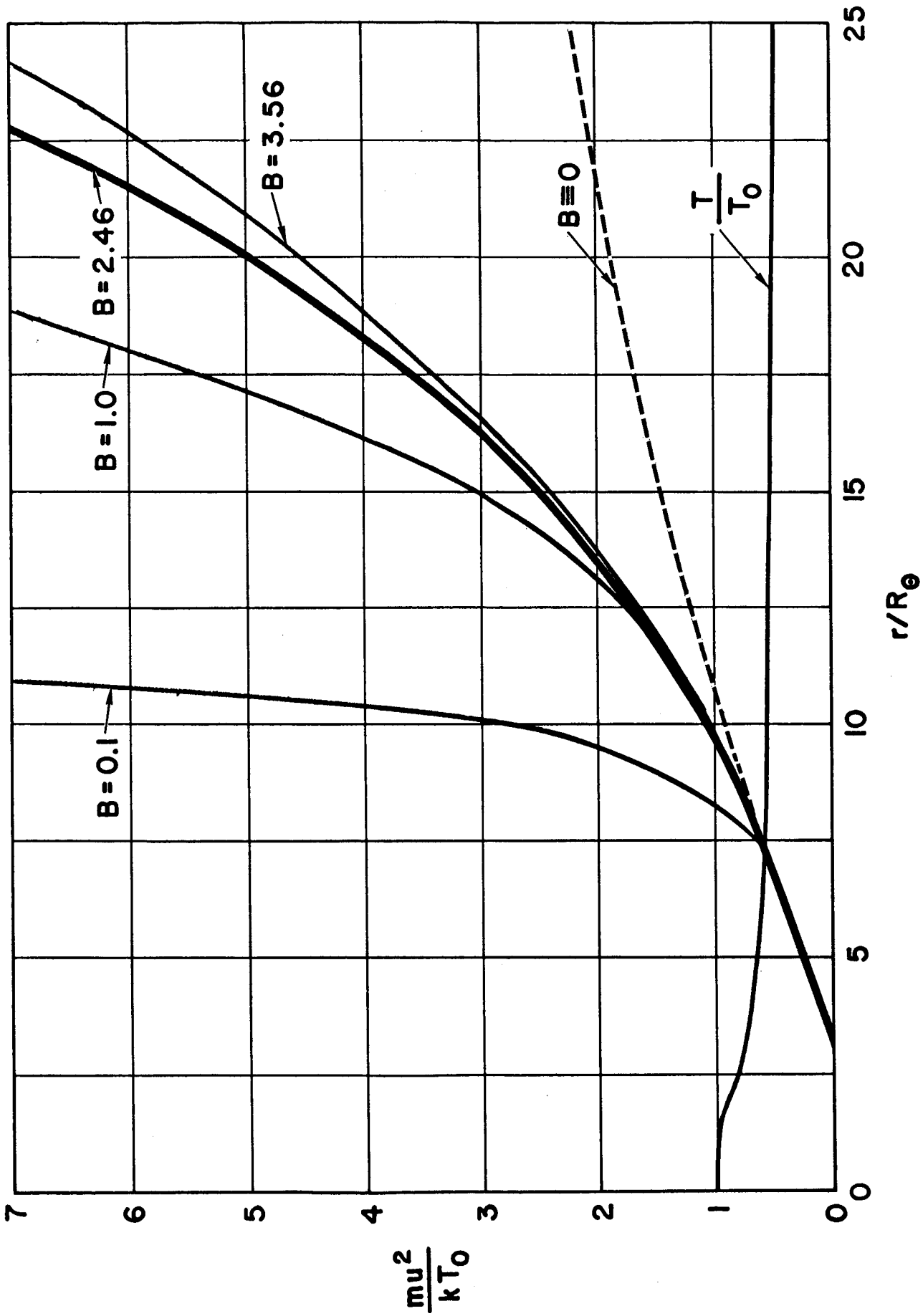

Figure 4